Available Online at http://www.journalajst.com

ASIAN JOURNAL OF SCIENCE AND TECHNOLOGY

ISSN: 0976-3376

Asian Journal of Science and Technology
Vol. 16, Issue, 01, pp. 13343-13352, January, 2025

RESEARCH ARTICLE

CONTRIBUTION TO THE DEVELOPMENT OF A METHOD FOR RECOGNIZING AND CLASSIFYING THE MALIGNANT AND BENIGN NATURE OF BREAST TUMOR USING A NEURAL NETWORK

Yeltongar NADJI[1*], Jerome MBAINAIBEYE[2] and Toussaint Gnonwa[3]

[1]Department of technical sciences, Faculty of Exact and Applied Sciences, University of N'Djamena, N'Djamena, Chad
[2]Department of technical sciences, Faculty of Exact and Applied Sciences, University of Moundou, Moundou, Chad
[3]Mother and Child Hospital, Faculty of Human Health Sciences, University of N'Djamena, N'Djamena, Chad

ARTICLE INFO

Article History:
Received 11th November, 2024
Received in revised form
11th December, 2024
Accepted 19th December, 2024
Published online 17th January, 2025

Keywords:
Breasttumour, recognition, classification, malignantcharacter, benigncharacter, neural network.

ABSTRACT

Breast cancer ranks first among the types of cancer affecting women worldwide. However, early detection can lead to effective treatment. Developing a system to make the decision on the benign or malignant nature of the tumour will help radiologists to establish a precise diagnosis in order to manage patients presenting the pathologies. The objective of this study is to develop a method that makes it possible to recognize the malignant or benign nature of breast cancer in a mammographic image, using the neural network. The method we developed is based on the neural network. Indeed, we extracted the characteristics of the mammographic images having undergone pre-processing and the detection of regions of interest by the multiscale product. These characteristics are extracted, in one hand by the Gray Level Co-occurrence Matrix (GLCM) and in the other hand the Gray Level Run Length matrix (GLRLM). The extracted characteristics constitute the data at the input of a neural network (the pattern net). The mammographic images from the MIAS database were used as a learning basis and recognition basis. This development allowed us to classify objects in a region of interest as malignant or benign. The results of the proposed method showed sensitivity, specificity and an area under the curve all equal to 1 for images labelled malignant and therefore cancerous. For images labelled benign, the sensitivity is equal to 0.8, the specificity is equal to 1, and the area under the curve is equal to 0.88. Thus, the results highlighted the effectiveness of the method we proposed. Compared to the results of the literature (recent state of the art), we can say that the method we proposed is the most efficient in terms of evaluation criteria. The most contributions of this work are the successful using of the characteristics of mammographic images (characteristics issues from the segmentation and multiscale product of 2-Dimensional continuous wavelet coefficient) extracted by GLCM and GLRLM and used as the input of a neural network to recognize and classify as benign or malignant the mammographic images.

Citation: Yeltongar NADJI, Jerome MBAINAIBEYE and Toussaint Gnonwa. 2025. "Contribution to the Development of a method for Recognizing and Classifying the Malignant and benign nature of breast tumor Using a Neural Network", *Asian Journal of Science and Technology*, 16, (01), 13343-13352.

Copyright©2025, Yeltongar NADJI, Jerome MBAINAIBEYE and Toussaint Gnonwa. *This is an open access article distributed under the Creative Commons Attribution License, which permits unrestricted use, distribution, and reproduction in any medium, provided the original work is properly cited.*

INTRODUCTION

In 2020, global breast cancer statistics recorded 2.3 million cases of the disease among women, including 685,000 unfortunate deaths [1]. It is the most common form of cancer in the world. The need for early and accurate diagnosis of the signs of this cancer such as microcalcifications plays a very important role in reducing the mortality rate [2]. Manual techniques used by radiologists fail due to the similarity in appearance of microcalcifications [2]. Therefore, the development of automated systems to help radiologists accurately diagnose breast cancers is necessary and the best way to screen for this cancer is mammography. Mammography is a process by which one can obtain images and through these images detect even small changes in the breast. However, the analysis and interpretation of mammographic images remains a difficult task due to noise, poor contrast and low limits etc. [3], [4]. To overcome this problem, the method of classifying images into healthy or cancerous images was considered. We chose the pattern recognition neural network for this and it is applied just after extracting features from mammographic images. The training of the network is carried out with the mini-MIAS base, which would be described in section 3. Several works have been published by researchers on different classification techniques, notably Sonia and colleagues [5] used texture energy measurement (LTEM) in conjunction with support vector machine (SVM) for classification purposes; Khan et al. [6] used the rotation-invariant "Local binary pattern" technique integrated into the uniform model to extract features, while using the SVM method for classification. The k-nearest neighbors (KNN) are also used in [7]. Each of these techniques has its performances but also its limitations. In this paper, we propose a new method for recognizing and classifying the malignant or benign nature of breast cancer using a neural network.

MATERIALS AND METHODS

Materials: We have used the Mammographic Image Analysis Society (MIAS) digital mammography database. MIAS, is an organization of researchers group interested by the work on mammography. This group is based in the United Kingdom and has produced a database of digital mammograms [8]. The x-ray films in the database were carefully selected from the UK National Breast Cancer Screening Program and scanned using a Joyce-Label scanning microdensitometer at up to 50 resolutions. µm x 50 µm; each pixel being coded on 8 bits. The database contains left and right breast images of 161 patients. In total, this basis has 322 images, belonging to three types, namely normal, benign and malignant. There were 208

normal images, 63 benign and 51 malignant (abnormal). Our choice of data for the evaluation of our method is this database because it presents several pieces of information about the anomaly, namely the class of the lesion, its location and its size. For our work, we have used the Intel(R) Core (TM) i5 CPU computer, 4 GB RAM memory and Matlab R2017b software.

METHODS

The proposed method includes different steps involving image-processing techniques [9] and the region of interest detection [10]. The ROI is then processed to extract a set of texture features using the Gray Level Concurrency Matrix (GLCM) and Gray Level Run Length Matrix (GLRLM).

Feature extraction: In 1973, Haralick introduced the gray level co-occurrence matrix (GLCM), which allows evaluating the distribution of gray levels in an image using second-order features [10]. GLCM characterizes the texture of an image by determining the frequency of apparition of pairs of pixels with specific intensities at a distance d and orientation θ [11]. Generally, we do not use the co-occurrence matrix directly but rather the characteristics calculated from it and the main ones of which are energy, entropy, contrast, correlation and homogeneity as follows and is illustrated by equations (4.1) to (4.5) respectively.

$$\text{Energy} = \sum_{i,j} P^2(i,j). \quad \ldots\ldots\ldots\ldots(1)$$

$$\text{Entropy} = -\sum_{i,j} P(i,j) \times \log_2(P(i,j)). \quad \ldots\ldots\ldots\ldots(2)$$

$$\text{Contraste} = \sum_{i,j=0}^{N-1} |i-j|^2 \sum_{i=1}^{N} \sum_{j=1}^{N} (P(i,j)). \quad \ldots\ldots\ldots\ldots(3)$$

$$\text{Correlation} = \sum_{i,j} \frac{(ij)\times P(i,j) - u_x u_y}{\sigma_x \times \sigma_y}. \quad \ldots\ldots\ldots\ldots(4)$$

$$\text{Homogeneity} = \sum_{i,j} \frac{P(i,j)}{1+(i-j)^2}. \quad \ldots\ldots\ldots\ldots(5)$$

Where $P(i,j)$ is the element of GLCM, N is the number of distinct gray levels in the GLCM. u_x, u_y, $\sigma_x et \sigma_y$ are respectively the mean and standard deviation of the marginal probabilities Px and Py given by equations (6) and (7), respectively.

$$P_x(i) = \sum_{j=1}^{N} P(i,j). \quad \ldots\ldots\ldots\ldots(6)$$

$$P_y(j) = \sum_{i=1}^{N} P(i,j). \quad \ldots\ldots\ldots\ldots(7)$$

Additionally, the mean, standard deviation, variance, skewness was calculated. The Gray Level Run Length matrix (GLRLM) was introduced by Galloway in 1975 and is based on the analysis of higher order statistical information [11]. The basis of the run length approach depends on calculating the number of gray levels of different lengths. This technique provides information on the length of pixels connected in a defined direction. Using the run length matrix, a minimum of seven distinct features can be derived in different directions, for example $(0^0, 45^0, 90^0, 135^0)$. These features include short-term focus, long-term focus, grayscale non-uniformity, track length non-uniformity, percentage range, low grayscale focus and high grayscale. These characteristics are illustrated by equations 4.8 to 4.14, respectively.

The short-term emphasis is defined by equation (8).

$$\frac{1}{N} \sum_{i,j} \frac{P(i,j)}{j^2}. \quad \ldots\ldots\ldots\ldots(8)$$

The long-term emphasis is defined by equation (9).

$$\frac{1}{N} \sum_{i,j} j^2 P(i,j). \quad \ldots\ldots\ldots\ldots(9)$$

The non-uniformity of the gray level is defined by equation (10).

$$\frac{1}{N} \sum_{i} \left(\sum_{j} P(i,j)\right)^2. \quad \ldots\ldots\ldots\ldots(10)$$

The non-uniformity of the length and range is defined by equation (11).

$$\frac{1}{N} \sum_{j} \left(\sum_{i} P(i,j)\right)^2. \quad \ldots\ldots\ldots\ldots(11)$$

The range percentage is defined by equation (12).

$$\sum_{i,j} \frac{1}{P(i,j)j}. \quad \ldots\ldots\ldots\ldots(12)$$

The low grayscale emphasis is defined by equation (13).

$$\frac{1}{N} \sum_{i,j} \frac{P(i,j)}{i^2}. \quad \ldots\ldots\ldots\ldots(13)$$

The emphasis of high gray levels is defined by equation (14).

$$\frac{1}{N} \sum_{i,j} i^2 P(i,j). \quad \ldots\ldots\ldots\ldots(14)$$

Where *P(i,j)* corresponds to the elements of GLRLM and *N* represents the total number of ranges.

The extracted texture features are then fed into a pattern recognition neural network (pattern net) [13]. This allows us to classify objects in regions of interest into either benign or malignant objects.

Classification: In our work, we have used the pattern recognition neural network (the "pattern net") for the classification of microcalcifications in digital mammographic images. According to the literature, there are various techniques to verify the reliability of classification performance evaluation. The best-known are: the peak signal-to-noise ratio (PSNR), the confusion matrix and the ROC (Receiver Operating Characteristic) curve, which are detailed in the sections below.

Confusion matrix: The confusion matrix illustrates the correlation between different performance indicators in the context of binary classification [14]. The authors of [14] mention that the four performance indicators are True Positive (VP), True Negative (VN), False Positive (FP) and False Negative (FN). They are usedto compare the expected results of the machine learning system with the confirmed labels obtained by biopsy. Considering these performance measures, we can calculate binary classification measures. We recall here the definitions of these four above performance indices:

- VP: tumor marked as malignant by a biopsy, which is also classified as malignant by the machine;
- FP: tumor marked as malignant by a biopsy, which is classified as benign by the machine;
- VN: tumor marked as benign by biopsy, which is also classified as benign by the machine;
- FN: tumor marked as benign by biopsy, which is classified as malignant by the machine.

This method uses three measures called sensitivity, specificity and precision, the definitions of which and the mathematical expressions allowing them to be calculated are presented below [15]:

- Sensitivity (equivalent to the true positive rate): proportion of positive cases that are correctly detected by the test. In other words, Sensitivity measures the effectiveness of the test when used on positive individuals. The test is perfect for positive individuals when the sensitivity is 1. However, that is equivalent to a drawing of lots when the sensitivity is 0,5. Finally, if it is less than 0.5, the test is underperforming and it is then useful to reverse the rule so that the sensitivity is greater than 0.5 (provided that this does not affect the specificity). The mathematical definition of sensitivity is given by:

$$Sensibilité = \frac{VP}{VP+FN} \quad \ldots\ldots\ldots\ldots(15)$$

Specificity (also called true negative rate): This is the proportion of negative cases that are correctly detected by the test. In other words,

specificity measures the effectiveness of the test when used on negative individuals. The test is perfect for negative individuals when the specificity is 1. However, that is equivalent to a drawing of lots when the sensitivity is 0,5. If it is less than 0.5, the test is underperforming and it is then useful to reverse the rule so that the specificity is greater than 0.5 (provided that this does not have an impact on the sensitivity). The mathematical definition is given by equation (16):

$$Spécificité = \frac{VN}{VN+FP} \quad \text{.....(16)}$$

Precision is a measure that determines the probability that the number of samples will be correctly classified. The mathematical definition is given by equation (17):

$$Précision = \frac{VP+VN}{VP+VN+FP+F} \quad \text{.....(17)}$$

The ROC curve: The ROC curve has been established in clinical biology for several years [16]. According to the authors of [16], it was in 1993 that Zweig et al. presented this statistical tool and its main applications [17]. They specified that this curve is included in the list published by the American Association for Clinical Chemistry grouping together the parameters to be studied during the evaluation ROC curve between January 2001 and December 2002 in the journal Clinical Chemistry [19]. The metrics used to define performance are sensitivity and specificity [20]. Sensitivity refers to the accurate classification of malignant mammographic masses by the learning system [21]. This curve is then plotted against (1 – specificity), which represents the misclassification of benign tumors by the diagnostic support system at different cutoff values [21]. ROC analysis is commonly used to determine the threshold value used as a criterion for testing medical diagnostic systems. By adjusting the cutoff value, it is possible to achieve an optimal balance between sensitivity and specificity, which is crucial for specific goals. Additionally, if the cost of not detecting a particular anomaly is significant to the test basis, the threshold value can be modified to achieve high sensitivity but lower specificity [16]. To visually represent the performance of a binary classification (Malignant/Benign), ROC curves may be displayed using the performance parameters "True Positive Rate (TVP)" and "False Positive Rate (FPR)" which can be calculated using the following functions:

TVP = Sensitivity (See equation 15).

TFP = 1 - Specificity (18)

(See equation 16).

RESULTS OBTAINED

Original images used for evaluation

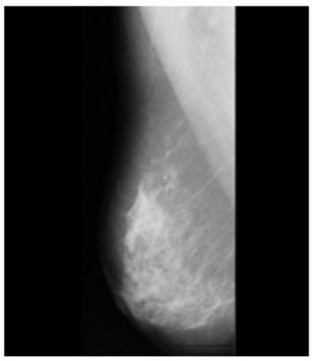

Fig. 1. mdb249 (diseased breast)

Fig. 2. mdb211 (diseased breast)

Fig. 3. mdb001 (breast without abnormality)

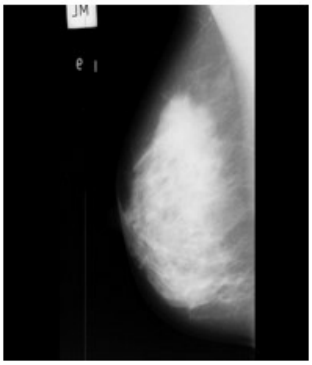

Fig. 4. Image mdb003 (breast without abnormality)

Feature Extraction Results

Tableau 1. Results of features extraction by GLCM for Image mdb249

	Direction Θ			
Features	0°	45°	90°	135°
Contrast	1.0015	4.0035	1.0015	7.9996 e-04
Dissimilarity	1.0007	2.0014	1.0007	7.9996 e-04
Homogeneity	0.5004	0.2002	0.5004	1.0003
Asymmetry moment	0.9970	0.9970	0.9970	0.9970
Energy	0.9985	0.9985	0.9985	0.9985
Maximal probability	0.9985	0.9985	0.9985	0.9985
Entropy	0.0055	0.0055	0.0055	0.0055
Average	1.0025	1.0024	1.0024	1.0024
Variance	6.7920e-04	6.7353e-04	6.7920e-04	6.7920e-04
Correlation	1	1	1	1

Tableau 2. Results of features extraction by GLCM for Image mdb211

	Direction Θ			
Features	0°	45°	90°	135°
Contrast	1.0026	4.0069	1.0026	0.0012
Dissimilarity	1.0014	2.0029	1.0014	0.0012
Homogeneity	0.5008	0.2004	0.5008	0.5008
Asymmetry moment	0.9947	0.9947	0.9947	0.9947
Energy	0.9974	0.9974	0.9974	0.9974
Maximal probability	0.9974	0.9974	0.9974	0.9974
Entropy	0.0091	0.0091	0.0091	0.0091
Average	1.0049	1.0049	1.0049	1.0049
Variance	0.0014	0.0014	0.0014	0.0014
Correlation	1.0000	1.0000	1.0000	1.0000

Tableau 3. Results of features extraction by GLCM for Image mdb001

Features	Direction Θ			
	0°	45°	90°	135°
Contrast	1.0000	4.0001	1.0000	2.672 e-05
Dissimilarity	1.0000	2.0000	1.0000	2.6729 e-05
Homogeneity	0.5000	0.2000	0.5000	1.0000
Asymmetry moment	0.9999	0.9999	0.9999	0.9999
Energy	1.0000	1.0000	1.0000	1.0000
Maximal probability	1	1	1	1
Entropy	2.0793 e-04	1.9876 e-04	1.9876 e-04	1.9876 e-04
Average	1.0001	1.0001	1.0001	1.0001
Variance	1.3363 e-05	1.3363 e-05	1.3363 e-05	1.3363 e-05
Correlation	1.0000	1.0000	1.0000	1.0000

Tableau 4. Results of features extraction by GLCM for Image mdb003

	Direction Θ			
Features	0°	45°	90°	135°
Contrast	1.0000	4.0000	1.0000	1.7183 e-05
Dissimilarity	1.0000	2.0000	1.0000	1.7183 e-05
Homogeneity	0.5000	0.2000	0.5000	0.5000
Asymmetry moment	1.0000	1.0000	1.0000	1.0000
Energy	1.0000	1.0000	1.0000	1.0000
Maximal probability	1.0000	1.0000	1.0000	1.0000
Entropy	1.1923 e-04	1.1923 e-04	1.1923 e-04	1.1923 e-04
Average	1.0000	1.0001	1.0001	1.0001
Variance	6.6819 e-06	6.6819 e-06	6.6819 e-06	6.6819 e-06
Correlation	1.0000	1.0000	1.0000	1.0000

Tableau 5. Results of features extraction by GLRLM for Image mdb249

Features	Direction Θ			
	0°	45°	90°	135°
Short Run Emphasis	0.1331	0.1554	0.2062	0.1583
Long Run Emphasis	5.1128e+05	1.0647e+06	4.1267e+05	1.0907e+06
Run Length no-uniformity	385.4118	645.1249	367.8495	657.7604
Run Percentage	0.0018	0.0013	0.0022	0.0012
gray level no-uniformity	3.3608e+03	1.7187e+03	1.3989e+03	1.6979e+03
Low Gray Level Run Emphasis	1.3242	0.7769	0.7212	0.7832
high gray level run emphasis;	19.6439	19.0704	23.5850	18.5610
short run low gray-level emphasis	1.2628e-06	3.7003e-07	6.8776e-07	3.7302e-07
short run high gray-level emphasis	1.8734e-05	9.0829e-06	2.2492e-05	8.8402e-06
long run low gray-level emphasis	2.9283e+03	5.8550e+03	3.6546e+03	5.6900e+03

Tableau 6. Results of features extraction by GLRLM for Image mdb211

Feature	Direction Θ			
	0°	45°	90°	135°
Short Run Emphasis	0.1518	0.1732	0.2162	0.1928
Long Run Emphasis	4.1702e+05	8.5246e+05	3.0833e+05	8.8750e+05
Run Length no-uniformity	357.6077	586.3642	363.6062	582.3506
Run Percentage	0.0022	0.0016	0.0030	0.0015
gray level no-uniformity	3.3137e+03	1.9718e+03	1.7182e+03	1.9024e+03
Low Gray Level Run Emphasis	1.1730	0.7224	0.6694	0.7344
high gray level run emphasis;	23.5911	23.4841	27.7786	22.5120
short run low gray-level emphasis	1.1187e-06	3.4407e-07	6.3839e-07	3.4979e-07
short run high gray-level emphasis	2.2498e-05	1.1185e-05	2.6492e-05	1.0722e-05
long run low gray-level emphasis	3.5834e+03	7.2851e+03	4.3332e+03	6.9701e+03

Tableau 7 Results of features extraction by GLRLM for Image mdb001

	Direction Θ			
Features	0°	45°	90°	135°
Short Run Emphasis	0.0500	0.0092	0.0148	0.0062
Long Run Emphasis	1.0153e+06	2.0295e+06	9.9785e+05	2.0473e+06
Run Length no-uniformity	977.9810	1.3716e+03	944.0638	1.3924e+03
Run Percentage	0.0010	7.0918e-04	0.0010	7.0442e-04
gray level no-uniformity	4.0419e+03	1.4495e+03	1.0248e+03	1.4493e+03
Low Gray Level Run Emphasis	1.9602	0.9867	0.9805	0.9900
high gray level run emphasis;	3.0380	2.0745	2.5760	1.8114
short run low gray-level emphasis	1.8694e-06	4.6996e-07	9.3512e-07	4.7151e-07
short run high gray-level emphasis	2.8973e-06	9.8807e-07	2.4567e-06	8.6272e-07
long run low gray-level emphasis	172.2770	348.1666	255.0216	262.8905

Tableau 8. Results of features extraction by GLRLM for Image mdb003

Features	Direction Θ			
	0°	45°	90°	135°
Short Run Emphasis	0.0479	0.0074	0.0152	0.0152
Long Run Emphasis	1.0268e+06	2.0519e+06	1.0128e+06	1.0128e+06
Run Length no-uniformity	992.9827	1.3943e+03	968.2254	968.2254
Run Percentage	0.0010	7.0347e-04	0.0010	0.0010
gray level no-uniformity	4.0608e+03	1.4493e+03	1.0245e+03	1.0245e+03
Low Gray Level Run Emphasis	1.9742	0.9906	0.9850	0.9850
high gray level run emphasis;	2.6737	1.7583	2.2121	2.2121
short run low gray-level emphasis	1.8827e-06	4.7182e-07	9.3940e-07	9.3940e-07
short run high gray-level emphasis	2.5498e-06	8.3744e-07	2.1096e-06	2.1096e-06
long run low gray-level emphasis	111.8123	245.6967	196.1422	196.1422

Classification results

Image mdb249

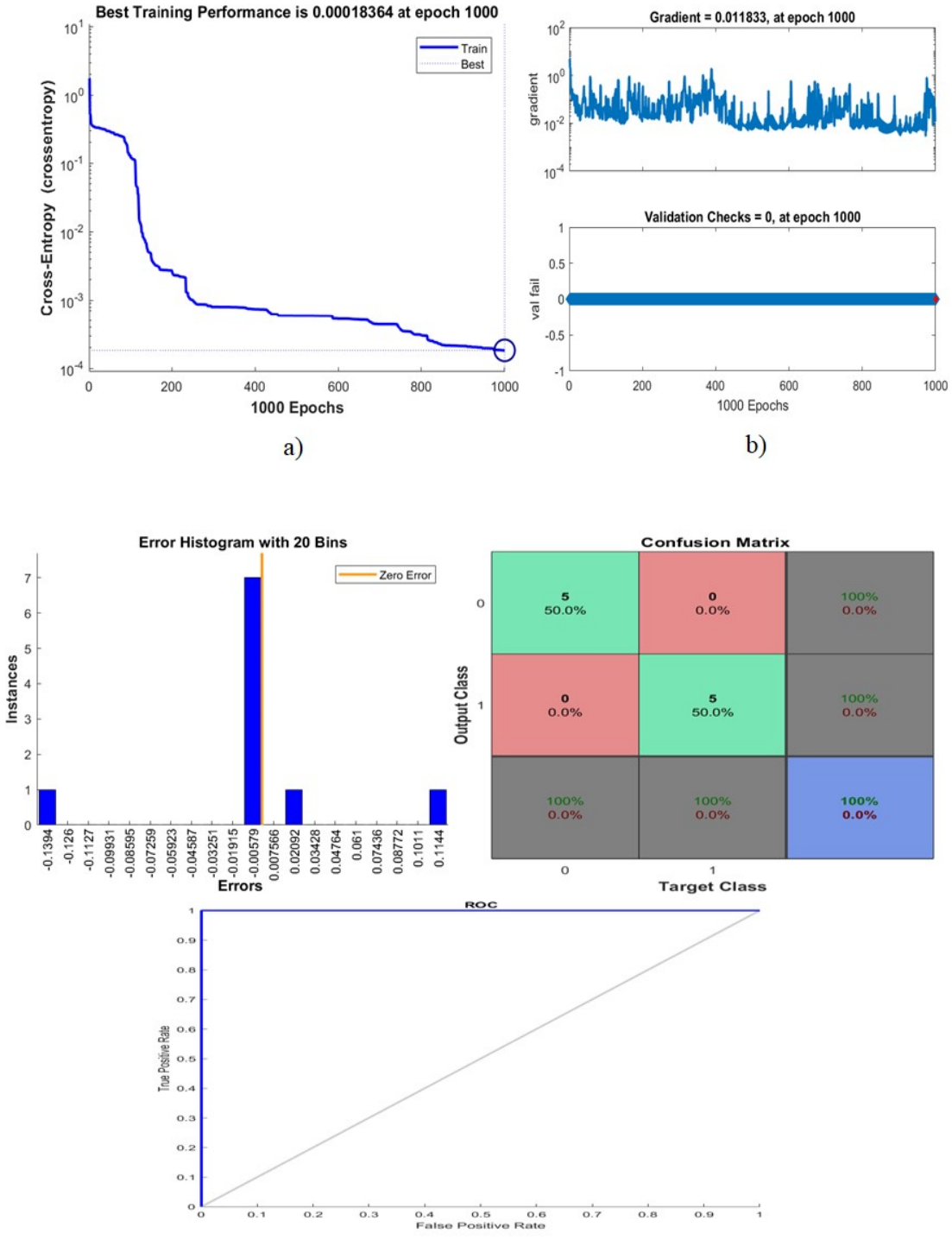

Fig. 5. a) Learning performance, b) Gradient and validation check, c) Error histogram, d) Confusion matrix and e) ROC curve

Image mdb211

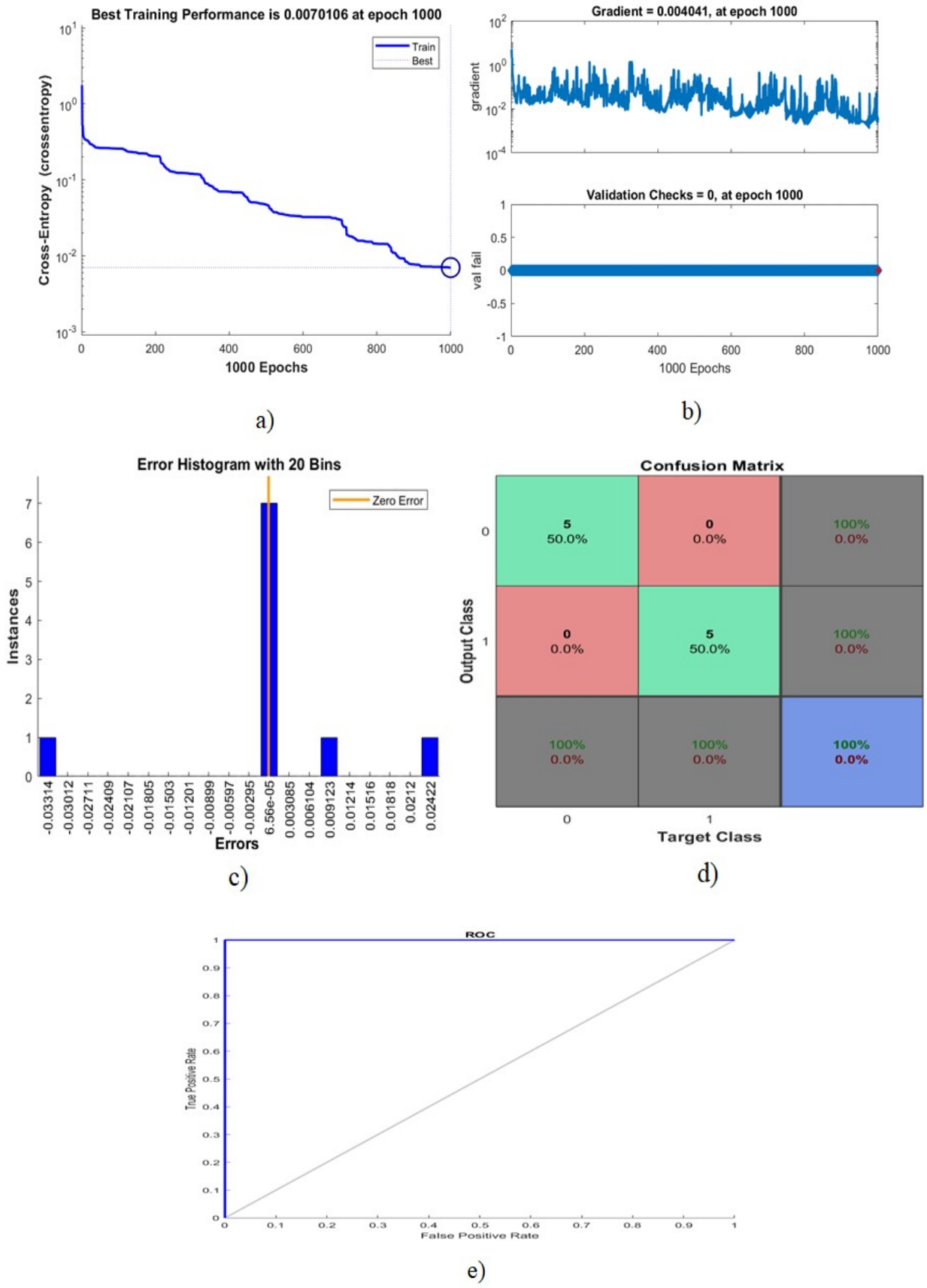

Fig. 6. a) Learning performance, b) Gradient and validation check, c) Error histogram, d) Confusion matrix and e) ROC curve

Image mdb001

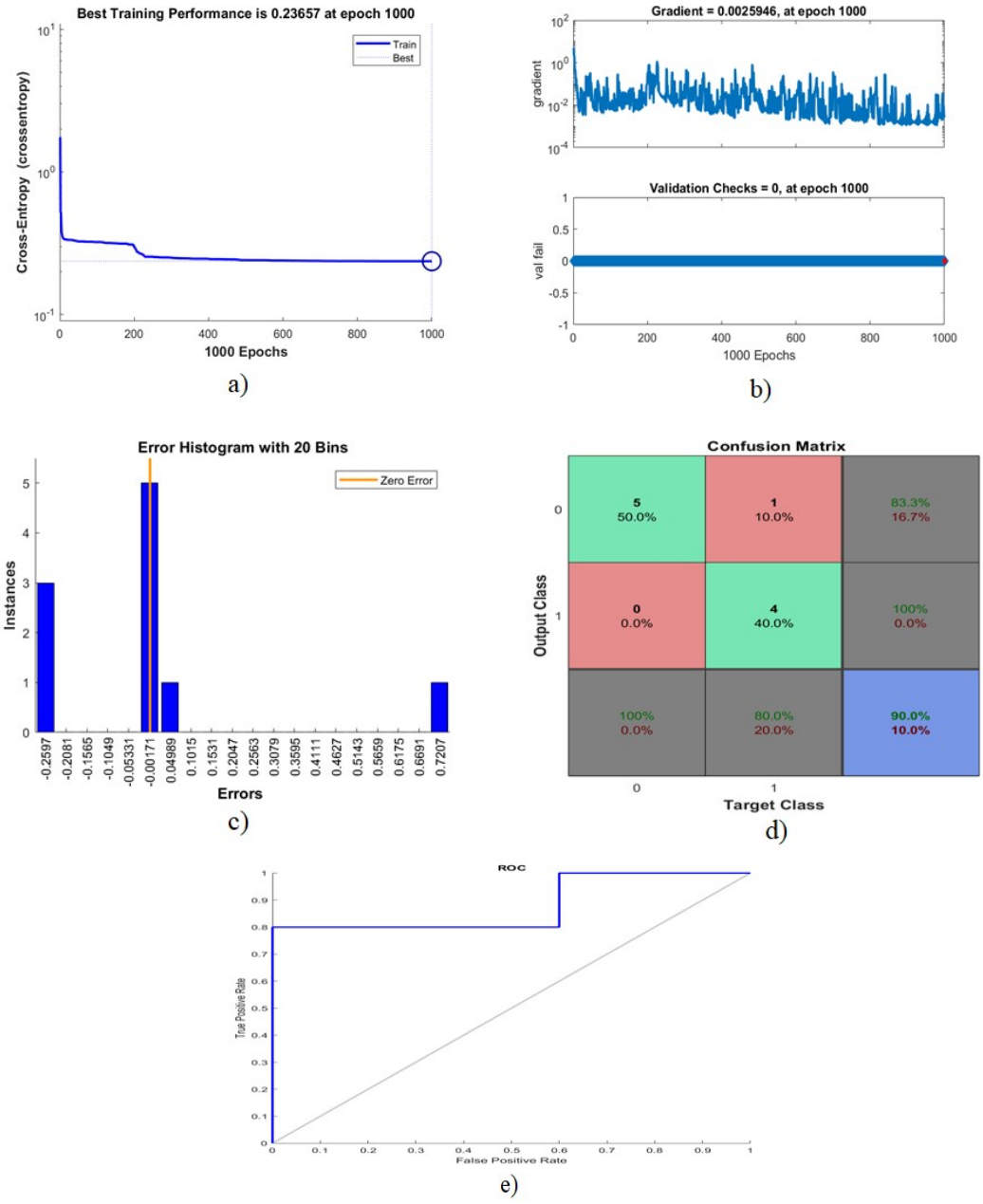

Figure 7: a) Learning performance, b) Gradient and validation check, c) Error histogram, d) Confusion matrix and e) ROC curve.

Image mdb003

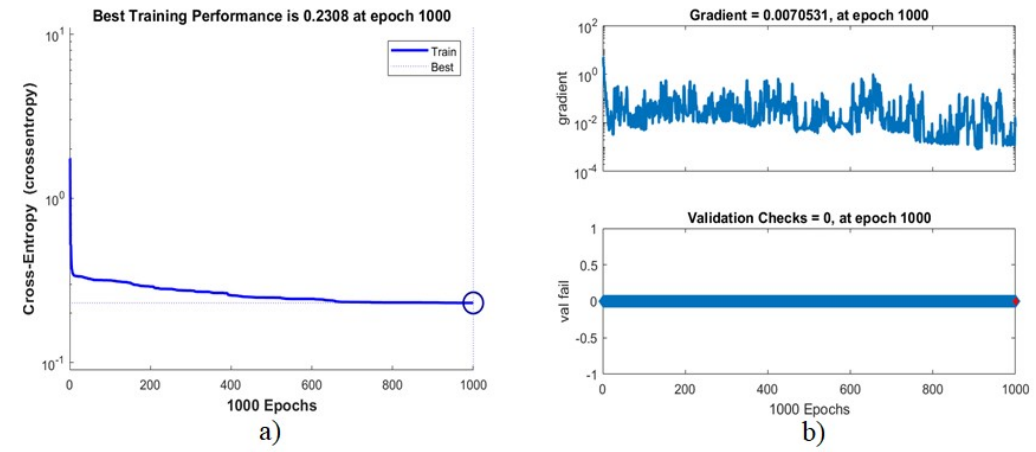

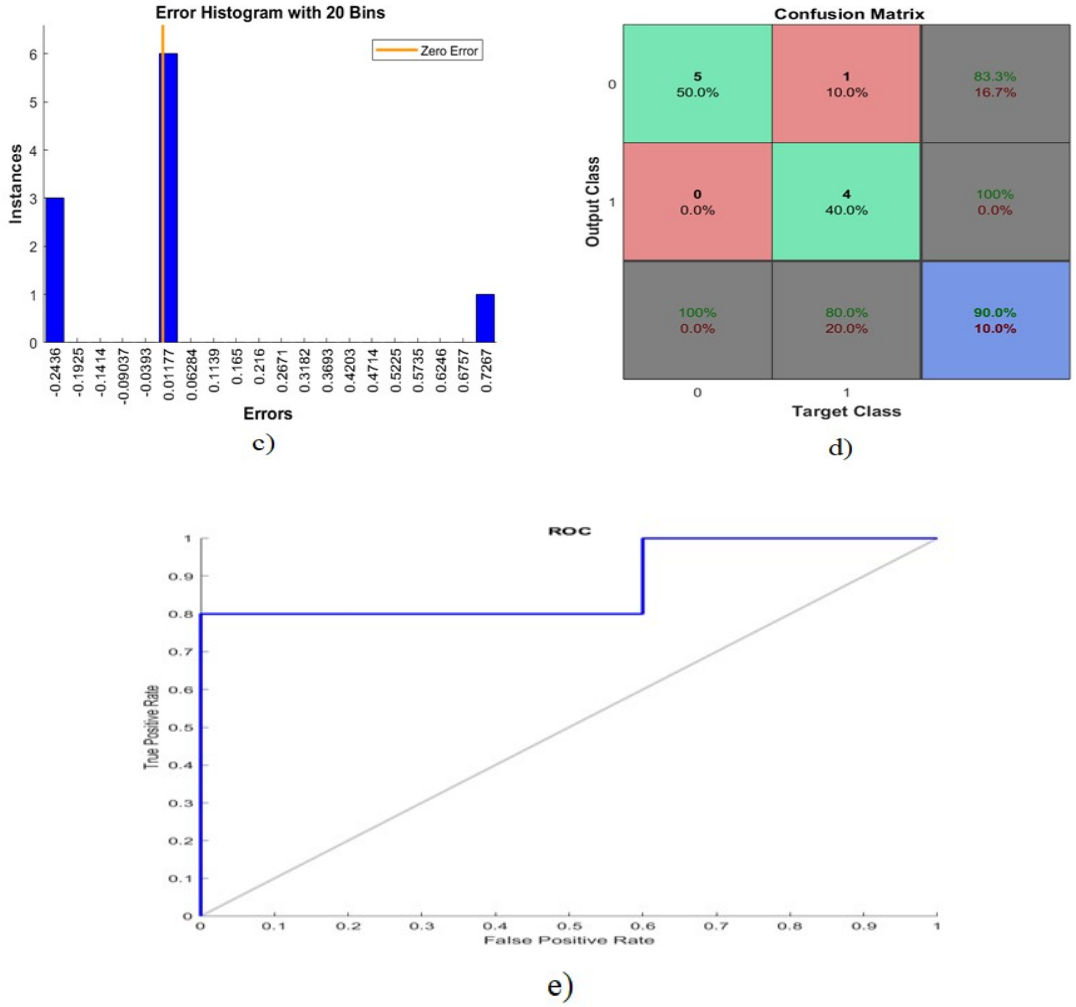

Fig. 8. a) Learning performance, b) Gradient and validation check, c) Error histogram, d) Confusion matrix and e) ROC curve

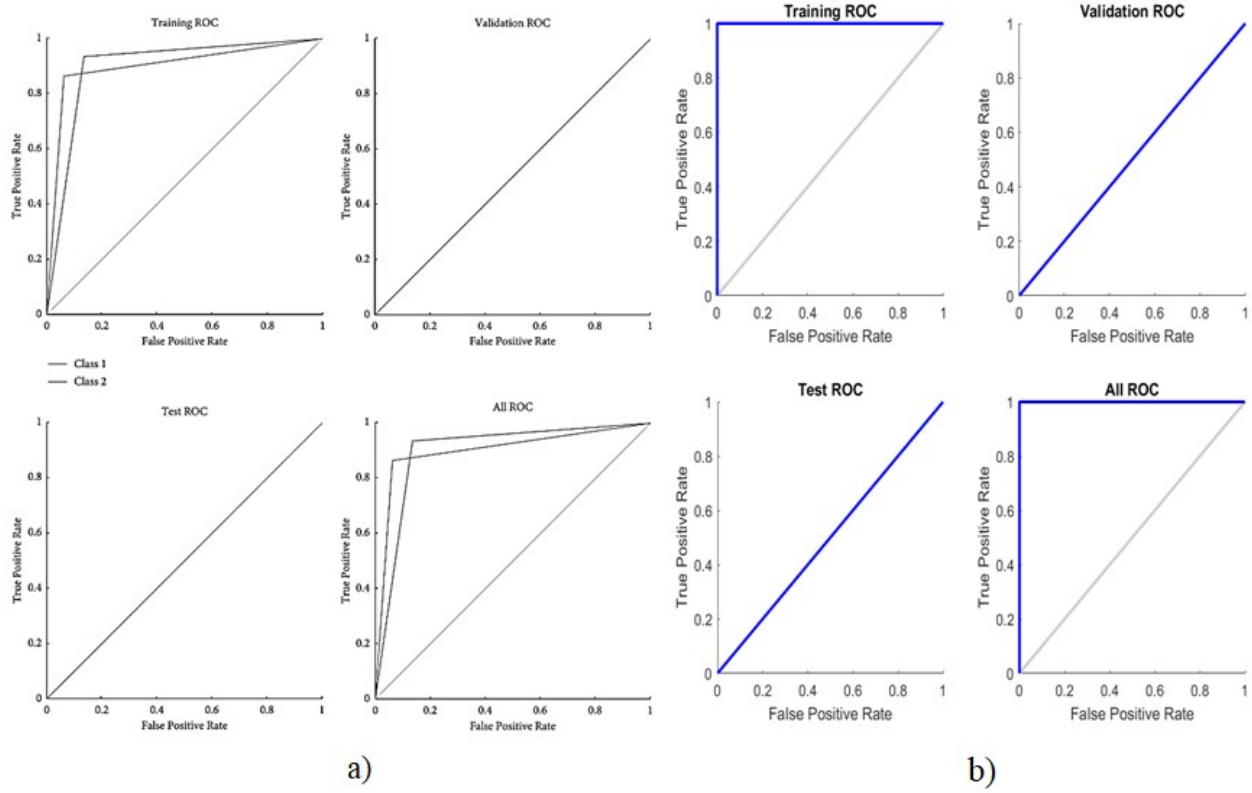

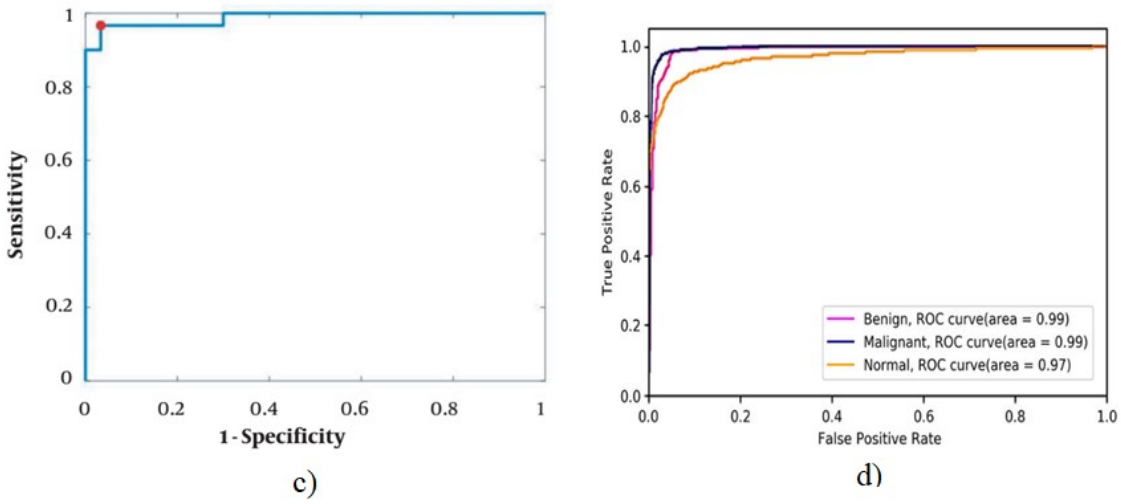

Fig.10. a) ROC curve from E. S. Pour et al., 2023, b) ROC curve from our method, c) ROC curve from Shiri Kahnouei M. et al., d) ROC curve from S. Akila Agnes et al.

Tableau 9. The results of comparing the proposed approach to the results of the literature

Reference	Date	Database	Sensitivity (%)	Specificity (%)	AUC
E. S. Pour et al. [22]	2023	MIAS	92.00	88%	0.8877
S. Punitha et al. [2]	2018	DDSM	98.1	97.8	-
ShiriKahnouei M et al. [23]	2022	CBIS-DDSM	96.7	96.7	98.8
S. AkilaAgnes et al [24]	2019	MIAS	92	94	0.99
Our method	2024	MIAS	100	100	1

DISCUSSIONS AND CONCLUSION

The results obtained by the proposed classification method with MIAS database images are encouraging. Indeed, we first extracted the texture characteristics of the images. Secondly, we introduced these characteristics into a pattern recognition neural network (the pattern net). This allowed us to classify objects from regions of interest and the results obtained by this approach show a very good classification rate. Thus, from Figure 5 a), b), c) and d) to Figure 8 a), b), c) and d), the results obtained from the classification by our method are presented. From all these figures we see that the best learning performance is achieved at a thousand (1000) epochs and a low gradient descent value. Error histograms at twenty levels (or periods) show zero error in all measurements. The confusion matrices clearly show that the network outputs are very accurate, as can be seen by the high numbers of correct classifications in the green squares (diagonal) and the low numbers of incorrect classifications in the red squares (outside diagonal). For malignant label images, most of the ROC curves pass through the coordinate point {0, 1} (Specificity = 1, Sensitivity = 1), the area under the associated curve is equal to 1 (see figures 5 e) and 6(e)). These results show that the system we proposed is very efficient and detects the points of discontinuity very well. For benign label images, most ROC curves do not reach the point with coordinates {0, 1}, they pass through a point closest to the upper left corner with coordinates {0, 0,8} (Specificity = 1, Sensitivity = 0.8), most of the area under the associated curve is equal to 0.88 (see Figures 7 e) and 8 e)). The system is also very efficient for this type of images. The proposed approach has a better receiver operating characteristic (ROC) curve and a larger area under the ROC curve (AUC), see Figure 10 a), b), c) and d) above. Table 3 presents the results of our method compared to those in the literature and shows that our method is better than other methods in terms of classification rate.

Acknowledgment

We would like to express our gratitude to the reviewers for their precise and succinct recommendations that improved the presentation of the results obtained.

Conflict of Interest: The authors declare no conflict of interest.

REFERENCES

Asma TOUIL, « Fusion collaborative de classifieurs : application a la détection de pathologies en mammographie », Thèse, Institut Supérieur de l'informatique et des technologies de la communication de Hammam Sousse, 2021, Unité de recherche : Latim (IMT Atlantique – France) et LATiS (Eniso, Sousse – Tunisie), Thèse N° : 2021IMTA0263.

Benhassine N E, « Contributions aux méthodes d'extraction de caractéristiques discriminantes pour la classification des images médicales », Thèse de Doctorat, Université Ziane Achour Djelfa, Algérie, Juillet 2019.

Chokri FERKOUS, Extraction des connaissances pour la segmentation d'images mammographiques, Université Badji Mokhtar-Annaba, Algérie, 2017.

Galloway, Mary M. "Texture analysis using gray level run lengths." Computer graphics and image processing 4.2 (1975): 172-179.

H. A. KHAN, A. AL HELAL, K. I. AHMED et R. MOSTAFA, « Abnormal mass classification in breast mammography using rotation invariant LBP, » in 2016 3rd International Conference on Electrical Engineering and Information Communication Technology (ICEEICT), IEEE, 2016, p. 1-5.

Haralick, Robert M., KarthikeyanShanmugam, and Its' HakDinstein. "Textural features for image classification." IEEE Transactions on systems, man, and cybernetics 6 (1973): 610-621.

https://fr.wikipedia.org/wiki/Reconnaissance_de_formes (consulter 19/02/2024).

https://www.who.int/fr/news room/fact-sheets/detail/breast-cancer# (consulted 16/03/2024).

ISSN: 1985-2304.

J. S. JEBAMONY et D. JACOB, « Classification of Benign and Malignant Breast Masses on Mammograms for Large Datasets using Core Vector Machines, » Current Medical Imaging, t. 16, no 6, p. 703-710, 2020.

Li, H. Zhang, S. Wang, Q. Zhu, R. Clinical value of mammography in diagnosis and identification of breast mass Pak. J. Med. Sci. 2016; 32, 1020–1025.

MarwaHmida, Reconnaissance de formes basée sur l'approche possibiliste dans les images mammographiques [Ph.D. thesis]. Université Bretagne Loire, IMT Atlantique, cotutelle Ecole Nationale d'Ingénieurs de Tunis ; 2017.

Nadji A. Yeltongar, Jerome B. Mbainaibeye and Toussaint C. Gnonwa, Detection of the Regions of Interest in Mammographic Images by the Multiscale Product and Segmentation Using the Continuous Wavelet Transform, *International Journal of Signal Processing System,* Vol.12, pp.7-11, 2024.

S. Punitha, A. Amuthan, K. Suresh Joseph, Benign and malignant breast cancer segmentation using optimized region growing technique, *Future Computing and Informatics Journal* 3 (2018) 348-358.

Y. Nadji, J. Mbainaibeye et G. Toussaint, Contribution to the Pre-processing Method for Image Quality Improving: Application to Mammographic Images, article, *International Journal of Image Processing (IJIP),* Volume (17): Issue (1): 2023 2

****